ADVANCED FUNCTIONAL MATERIALS
www.afm-journal.de

Creating Effective Nanoreactors on Carbon Nanotubes with Mechanochemical Treatments for High-Areal-Capacity Sulfur Cathodes and Lithium Anodes

*Gang Yang, Jian Tan, Ho Jin, Young Heon Kim, Xinyu Yang, Dong Hee Son, Sangjung Ahn, Hongcai Zhou, and Choongho Yu**

Li-S batteries can potentially deliver high energy density and power, but polysulfide shuttle and lithium dendrite formations on Li metal anode have been the major hurdle. The polysulfide shuttle becomes severe particularly when the areal loading of the active material (sulfur) is increased to deliver the high energy density and the charge/discharge current density is raised to deliver high power. This study reports a novel mechanochemical method to create trenches on the surface of carbon nanotubes (CNTs) in free-standing 3D porous CNT sponges. Unique spiral trenches are created by pressures during the chemical treatment process, providing polysulfide-philic surfaces for cathode and lithiophilic surfaces for anode. The Li-S cells made from manufacturing-friendly sulfur-sandwiched cathodes and lithium-infused anodes using the mechanochemically treated electrodes exhibit a strikingly high areal capacity as high as 13.3 mAh cm^{-2}, which is only marginally reduced even with a tenfold increase in current density (16 mA cm^{-2}), demonstrating both high "cell-level" energy density and power. The outstanding performance can be attributed to the significantly improved reaction kinetics and lowered overpotentials coming from the reduced interfacial resistance and charge transfer resistance at both cathodes and anodes. The trench–wall CNT sponge simultaneously tackles the most critical problems on both the cathodes and anodes of Li-S batteries, and this method can be utilized in designing new electrode materials for energy storage and beyond.

1. Introduction

The recent high demands for low-cost and high-density energy storage have turned the researchers' attention from traditional Li-ion batteries used in portable electronics and electric vehicles to other batteries based on different chemistry due to the unsatisfactory energy density of Li-ion batteries particularly for large-scale applications like transportation and stationary energy storage.[1] On the cathode side, conversion chemistry has shown great promise for replacing the intercalation chemistry of Li-ion batteries. Conversion-type cathode materials like sulfur and oxygen can provide 2567 and 3505 Wh kg^{-1}, respectively, compared to 387 Wh kg^{-1} of the intercalation-type $LiCoO_2$ cathode.[2] In particular, Li-S batteries have attracted rapidly increasing attention and substantial progresses have recently been made to alleviate their inherent problems like lithium polysulfide dissolution and shuttle, insulating nature of the end products, and volume variations of sulfur cathode during cycling.[3]

As a result, the specific capacity and cycling performance have been markedly improved when the areal loading of sulfur (active material) is low. The energy density based on the mass of sulfur only (not whole cathode or battery pack) has been good enough to beautify researchers' results, but the low sulfur loading has negated the high-energy-density merit of Li-S batteries, resulting in no improvement in the actual energy density of the "cell" or "battery pack" compared to the Li-ion batteries. To have a high "cell-level" energy density, the areal loading of sulfur needs to be increased to ≈10 mg cm^{-2} or higher, compared to typical literature values

G. Yang, J. Tan, Prof. C. Yu
Department of Mechanical Engineering
Texas A&M University
College Station, TX 77843, USA
E-mail: chyu@tamu.edu
H. Jin, X. Yang, Prof. D. H. Son, Prof. H. Zhou
Department of Chemistry
Texas A&M University
College Station, TX 77843, USA
Dr. Y. H. Kim, Dr. S. Ahn
Korea Research Institute of Standards and Science
Daejeon 34113, Republic of Korea
Prof. C. Yu
Department of Materials Science and Engineering
Texas A&M University
College Station, TX 77843, USA
The ORCID identification number(s) for the author(s) of this article can be found under https://doi.org/10.1002/adfm.201800595.

DOI: 10.1002/adfm.201800595

(commonly less than ≈1 mg cm^{-2} and a few of them reaching up to 3 mg cm^{-2}).[4]

On the other hand, the traditional graphite anode has been regarded as another bottleneck toward a high "cell-level" energy density due to its low theoretical capacity (370 mAh g^{-1}).[5] Lithium metal has been acknowledged as the ultimate anode material since it offers the highest theoretical capacity (3860 mAh g^{-1} and 2061 mAh cm^{-3}).[6] Li metal anodes for rechargeable batteries date back to 1970s when the first Li rechargeable batteries were built, but they were impractical due to short life cycles and safety issues mainly caused by dendrite formations. To mitigate the problem, various strategies such as electrolyte additives, solid-state electrolytes, and stabilization of solid electrolyte interphase (SEI) layers have been reported in the literature but have never been realized in practical applications.[6a,b,7] The pure Li metal anode suffers from the infinite dimension change during Li plating (i.e., Li ions are reduced and deposited on the anode) and stripping (i.e., Li metal are oxidized and dissolved into electrolyte). This often inevitably breaks the SEI layer, which can cause irreversible loss of active materials, and forms dendrites during preferential Li depositions on a flat and nonporous surface.

Here we report unique spiral trench features on the wall of the carbon nanotube (CNT) in a 3D sponge-like CNT-based framework, which has largely suppressed the aforementioned problems on both cathode and anode. The trenches act as nanoreactors, hosting polysulfides and lithium as well as shortening the diffusion length of active materials to improve reaction kinetics. We have developed a novel one-step mechanochemical method to create nanoreactors with functionalized surfaces, which have converted the surface of the pristine CNT (P-CNT) to strongly polysulfide-philic and lithiophilic surfaces. While considerable reduction in the overpotentials during charge and discharge surfaces effectively promoted the reactions for polysulfides and lithium, the pores in the sponge-like framework provided enough spaces to accommodate the problematic volume changes. The highly effective sulfur/lithium dual host resulted in the highest areal capacity of 10.3 mAh cm^{-2} after 100 cycles among those available in the literature, to the best of our knowledge, with the high areal loading of sulfur (10 mg cm^{-2}) at a high current density of 5 mA cm^{-2}. Furthermore, the capacity was minimally decreased despite the tenfold increase of the current density from 1.6 to 16 mA cm^{-2}, suggesting high "cell"-level power and energy densities.

2. Results and Discussion

To synthesize trench–wall carbon nanotube sponge structures, we have used a porous sponge-like 3D CNT structure as a base material, as illustrated in **Figure 1**a (also see a photograph in Figure S1a, Supporting Information).[8] The highly conducting CNTs are connected without binders, providing excellent electron paths and minimizing inactive materials. The porous structure is also ideal as a polysulfide reservoir.[9] The pristine CNT is expected to have lightly physisorbed and/or chemisorbed oxygen due to the exposure to air but the surface is mainly composed of a pristine graphitic layer (Figure 1b), which has a relatively small binding energy with polysulfides.[10] Despite the relatively weak binding (Figure 1c), this would remain as an effective strategy, provided the areal loading of sulfur is kept low—less than a few mg cm^{-2}. However, a high areal loading of sulfur requires more favorable and larger surfaces to promote the adsorption of polysulfides so as to impede the polysulfide shuttle resulted from the increased amount of polysulfides.

Here we have created trench-like sub-structures on the wall of CNTs using a mechanochemical method (Figure 1d,e). The highly oxidative exfoliating agent made of $KMnO_4$ and H_2SO_4 unzipped the graphitic layers, leaving carboxyl groups at the edge of the graphitic layers.[11] To create the trench–wall structure, we found that it is necessary to apply mechanical forces to the CNT during the bond cleavage process, which has been implemented by the pressure difference between the two sides of the CNT sponge in the vacuum filtration setup. It is the first time, to the best of our knowledge, to create trench-like sub-structures on a CNT, suggesting a new way of functionalizing and engineering a multiwall CNT. When CNTs are completely unzipped, the separated graphitic layers loose electrical contacts with neighboring structures. Here the cylindrical sponge structure was maintained after creating the nanotrenches, ensuring excellent electrical conduction through the porous CNT sponge structure (Figure S1b, Supporting Information).

The cleavage processes are conceptually illustrated in Figure 1g–i with only two outer walls for clarity. The trench wall feature would be initiated at the sites with weaker bonding or defects (Figure 1g) by opening C—C bond with the formation of manganate ester[11] (Figure 1h) along the $KMnO_4/H_2SO_4$ solution path because the bonding energies between MnO_4^{-1} anion and carbon in CNT were found to be lower than that of the separated state.[11] After a C—C bond is cleaved, the neighboring bonds are stretched and the cleavage process continues to the inner walls and along weaker bonding sites (Figure 1i). The unzipping process would end when the oxidizing anion is depleted in the trench. Increasing vacuum filtration pressure could promote the accessibility of the oxidizing anion into the deeper sites in the multiwalls of CNT, resulting in deeper and wider trenches.

To identify the role of the mechanical force in creating the nanotrenches, three different vacuum pressures 11, 48, and 62 kPa were used (labeled as MC11-CNT, MC48-CNT, and MC62-CNT, respectively). Figure 1j–l shows the transmission electron microscope (TEM) images of the mechanochemically treated CNT with the three different vacuum pressures. With higher pressures, the mechanical forces on CNTs with the etching solution are stronger (i.e., force = pressure × area), so the trench width was broadened from ≈5 nm on MC11-CNT to ≈30 nm on MC48-CNT and ≈60 nm on MC62-CNT. When the CNT sponge was immersed in the chemical solution without the pressurized filtration process (labeled as C-CNT), trench-like features were not identified from C-CNT. TEM images showed that the chemical treatment introduced only surface disorder (Figure S2b, Supporting Information) compared to the ordered graphitic layers in pristine CNTs (Figure S2a, Supporting Information). The contrast between inner and outer walls of C-CNT could be attributed to the oxidation of surface graphitic layers (5–10 nm from the outermost layer). This

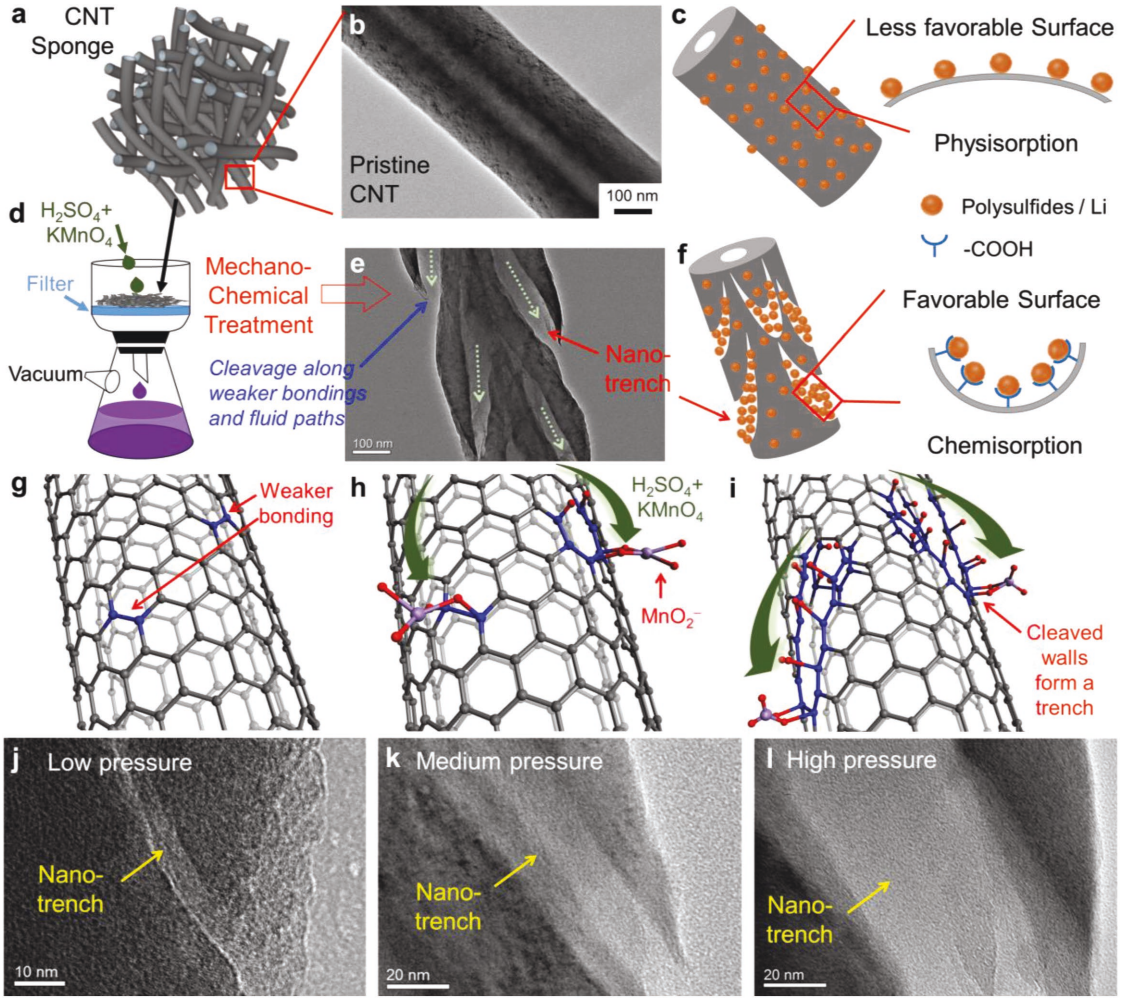

Figure 1. Illustrations of a) a pristine CNT sponge and d) a mechanochemical treatment process of the CNT sponge. TEM images of b) a pristine CNT sponge and e) a mechanochemically treated CNT sponge. Illustrations conceptually showing the interactions c) between the pristine CNT and polysulfides (or Li) as well as f) between the mechanochemically treated CNT and polysulfides (or Li). g) Illustration representing a CNT (grey sphere: carbon) with weaker bondings or defect sites (in blue). h) Illustration showing the cleaveage process initiated by the formation of MnO_2^- on the CNT along the $KMnO_4/H_2SO_4$ solution paths, leaving carboxyl groups (red sphere: oxygen; purple sphere: manganese) on the CNT. i) Both the outer and inner walls are cleaved continuously, resulting in treches on the CNT. TEM images of mechanochemically treated CNTs with vacuum pressures of j) 11 kPa (MC11-CNT), k) 48 kPa (MC48-CNT), and l) 62 kPa (MC62-CNT).

suggests that the mechanical force applied simultaneously with the chemical etching solution is essential to creating the unique trench-embedded CNT, as illustrated in Figure 1e. The pressure is likely to enforce the exfoliating agent to penetrate into the inner walls of CNTs by breaking the relatively weak carbon–carbon bonds along the fluid path. This process would also explain wider and deeper trenches when a higher vacuum pressure was applied.

The trench structures gave rise to larger D/G ratios in the Raman spectra compared to that of the pristine CNT (**Figure 2**a). According to the Fourier transform infrared spectroscopy (FTIR) results (Figure 2b), the prominent C=O peak from −COOH appeared from the mechanochemically treated CNT sponge. X-ray photoelectron spectroscopy results (Figure S3, Supporting Information) display oxygen 1s corresponding to C=O and −OH in the carboxyl group became prominent after the chemical treatment compared to the pristine CNT whose oxygen is mainly from adsorption. For the chemically treated samples, O at% with respect to C at% was raised as more intense treatment was performed, suggesting the increasing concentration of the carboxyl group (Table S1 and Figure S3, Supporting Information).

We tested the effectiveness of the mechanochemical treatment in adsorbing the polysulfides by immersing a piece of a P-CNT and MC48-CNT into a polysulfide solution (Figure 2c). The reddish color of the pure polysulfide solution almost disappeared with MC48-CNT but P-CNT marginally altered the color, suggesting a much superior polysulfide adsorption for MC48-CNT. UV–vis spectra were also taken for these three solutions. The MC48-CNT solution showed a marked intensity reduction of the peaks associated with polysulfides. It appears that the carboxyl group and the extended surface areas in the trench played a key role in adsorbing the polysulfides, as comparatively illustrated in Figure 1c,f. Computational studies[10] have also shown

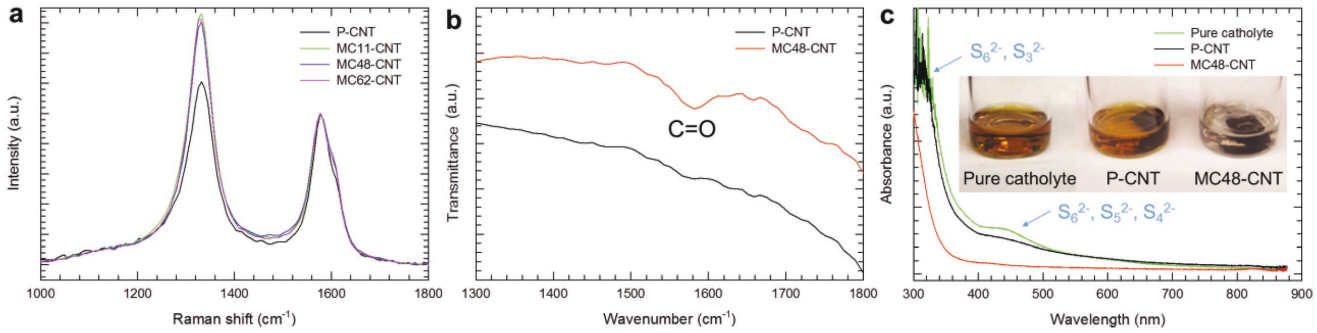

Figure 2. a) Raman spectra of a P-CNT sponge and the mechanochemically treated CNT sponges. b) FTIR spectra of P-CNT and MC48-CNT. c) UV–vis spectra and photos (inset) of pure polysulfide catholyte solutions without CNTs (left) and with P-CNT (middle) and MC48-CNT (right).

that the carboxyl group on graphitic carbon could increase the binding energy with polysulfides and it could also intensify the binding energy for lithium.

The trench–wall CNT sponges were used for both cathode and anode using simple and facile fabrication methods for testing. For cathode fabrication, sulfur was simply sandwiched between two pieces of the CNT sponges and then pressed in an ambient condition. This binder-free and trench–wall CNT cathode allowed us to remarkably increase the sulfur loading (10 mg cm^{-2}). Furthermore, this process is manufacturing friendly by eliminating the need for an inert environment as well as typically used thermal infusion processes for sulfur. The anode was prepared by thermally infusing lithium into MC48-CNT (Li@MC48-CNT). The molten lithium was spontaneously infused into the MC48-CNT. The highly porous structure and its surface with a high affinity to lithium owing to the high binding energy between lithium and carbonyl groups[12] are ideal for accommodating a large amount of lithium. The nanoscale trench structure could generate a capillary action, promoting the intake of molten lithium.

For self-comparative studies, we made four different sets of cathode and anode "pairs". First sulfur-loaded pristine CNT sponge cathode along with lithium metal anode (S@P-CNT//Li) was prepared as our reference. To identify the influence of the mechanochemical treatment on the performance, CNT sponges treated with two different vacuum pressures with lithium metal anode (S@MC11-CNT//Li and S@MC48-CNT//Li) were tested. Lastly, both cathode and anode were prepared using the mechanochemically treated CNT sponge (S@MC48-CNT//Li@MC48-CNT).

Figure 3a shows the areal capacity of the four different cells to evaluate the "cell"-level performance. It is worth noting that, in actual battery operation, the areal capacity delivered at a high current density is more important than the specific capacity (based on sulfur mass) that indicates the degree of sulfur utilization. The best performance was observed from the cell made of MC48-CNT for both cathode and anode (S@MC48-CNT//Li@MC48-CNT). This cell displayed a large areal capacity of 12.1 mAh cm^{-2} at the beginning and a stable cycling for longer than 250 cycles at a high current density of 4.8 mA cm^{-2}. When Li metal was used as anode instead of MC48-CNT, the capacity was similarly maintained but the cycling was suddenly stopped at the 145th cycle, which is typically caused by the internal short-circuit.[12] The longer cycling with Li@MC48-CNT anode can be ascribed to the outstanding lithium host with its lithiophilic surface promoting uniform lithium deposition and its porous structure accommodating dendrites, if any, in the void of the porous structure. In fact, all the other cells using Li metal anode could not survive more than 170 cycles under this harsh cycling condition. This internal short-circuit becomes prominent when the sulfur loading and current density are high because a large volume of lithium is repeatedly stripped and deposited, increasing the chance of forming lithium dendrites on anode.

When the trench structure was lightly formed (S@MC11-CNT//Li), the capacity was reduced to 8.5 mAh cm^{-2} at the initial cycle, indicating that the trench plays an important role in utilizing sulfur and suppressing the polysulfide shuttle. The polysulfides surrounded by the trench would have relatively short diffusion lengths, and the high polysulfide affinity could promote evenly distributed redox reactions along the trench wall, minimizing a bulk or nonuniform deposition of the insulating end products such as sulfur and Li_2S_2/Li_2S. The lower capacity from the pristine CNT (S@P-CNT//Li) confirms the effectiveness of the trenches in increasing the areal capacity.

We compared the "cell"-level performance of our cell (S@MC48-CNT//Li@MC48-CNT) with those of other Li-S cells in literature by plotting the areal capacity near 100th cycle versus the areal current density (Figure 3b). Here we compared the performance near the 100th cycle rather than the highest performance (or capacity) because the highest is often observed only at the first few cycles, which does not have much value in practice. We categorized the literature based on the cathode material in Figure 3b: (1) CNT (data labeled as A,[13] B,[14] C,[15] D,[16] E,[17] and F[18]); (2) graphene or graphene oxide (data labeled as G,[19] H,[20] I,[21] and J[22]); (3) mixture of CNT and graphene (or graphene oxide) (data labeled as K,[23] L,[24] and M[25]); and (4) others like polymers or inorganic metal-based materials (data labeled as N,[26] O,[27] P,[28] Q,[29] R,[4a] S,[30] T,[31] and U[32]). The upper part of Figure 3b implies a high "energy" stored in the cell, and the right-hand side of the Figure 3b suggests the cell can deliver a high "power" (or discharge rate). The data point corresponding to our Li-S cell equipped with trench–wall CNTs on both cathode and anode appears on the upper-right corner (10.3 mAh cm^{-2} and 4.8 mA cm^{-2} at the 100th cycle), outperforming the cell-level performances in the literature whose data points appear on the left and bottom corner.

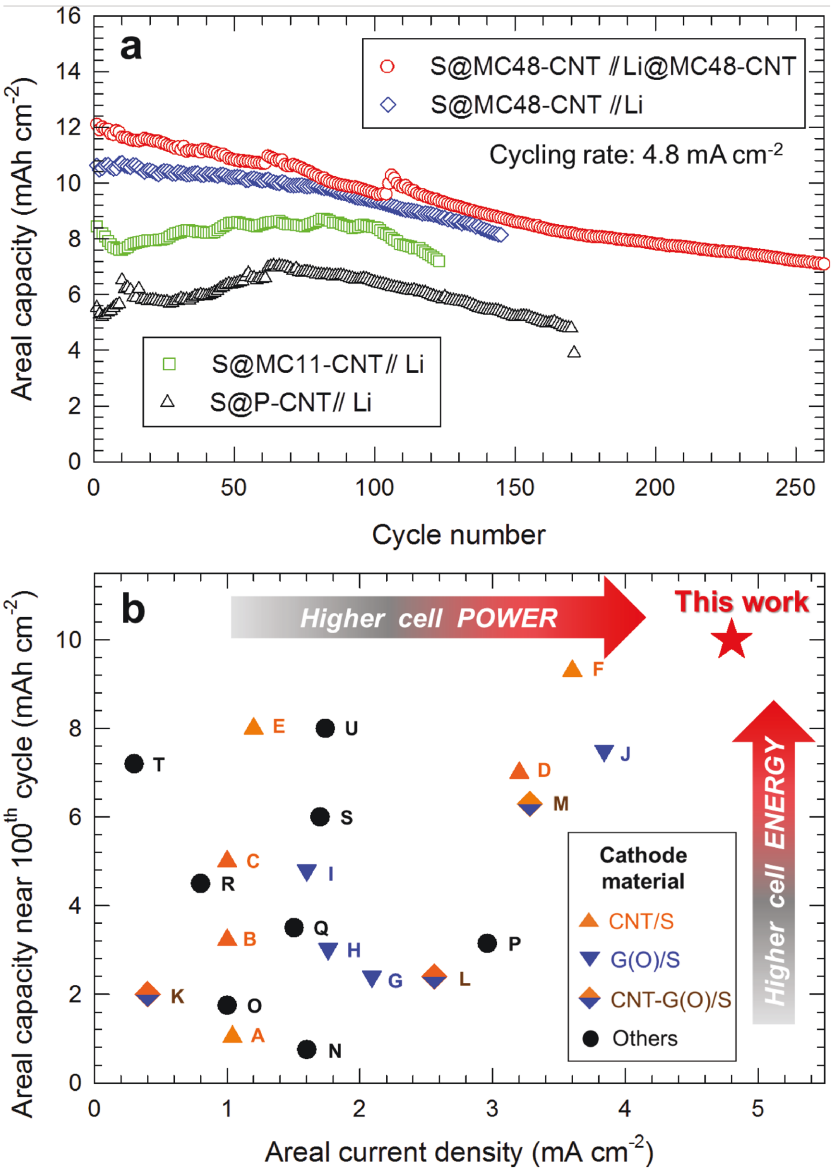

Figure 3. a) Areal capacity versus cycle number for four different cell configurations with a cathode made of MC48-CNT, MC11-CNT, or P-CNT and an anode made of MC48-CNT or Li. All cells had an areal sulfur loading of 10 mg cm^{-2} and were cycled under 4.8 mA cm^{-2}. b) Areal capacity (related to "cell"-level energy density) near the 100th cycle and areal current density (related to "cell"-level power density) of the S@MC48-CNT//Li@MC48-CNT cell (red star) and those of various Li-S cells in literature. The literature values are categorized based on cathode materials: CNT and sulfur (orange upper triangles); graphene (oxide) and S (blue lower triangles); CNT, graphene (oxide), and sulfur (orange/blue diamond); and others (black circles).

To validate the role of the trench, sulfur-loaded MC48-CNT (S@MC48-CNT) cathode after cycling was inspected under TEM (**Figure 4**a). Figure 4b shows energy dispersive spectroscopy (EDS) line scan results along the radial direction crossing the trench. The intensity of sulfur was sharply raised at the position where that of carbon was decreased (marked with an arrow), suggesting sulfur is rich along the trench. We also found crystalline Li_2S domains of a few nanometers in size when inspecting the cycled S@MC48-CNT cathode. We randomly picked three regions near the trench (Figure 4c) and the outer graphitic layer (Figure 4d). More details can be found from the enlarged images in Figures S4–S6 (Supporting Information). After performing the Fourier transformation, diffraction patterns corresponding to the crystal structure of Li_2S (Figure 4e,f and Figure S7, Supporting Information) were identified. The TEM results suggest that the exfoliated graphitic layers could attract polysulfides since Li_2S is converted from the reduction of polysulfides. The edge of graphitic layers can be highly functionalized after treatment with oxidizing agents,[11] so the trench walls can serve as a nanoscale polysulfide reactor like Figure 1f. The unique trench–wall features on CNT would have played essential roles in hosting a large amount of polysulfides and lithium as well as assisting electrochemical reactions.

To further analyze the origin of the outstanding cell performance, electrochemical impedance spectroscopy for the three representative cells (S@MC48-CNT//Li@MC48-CNT; S@MC48-CNT//Li; S@P-CNT//Li) at the 10th and 50th cycles was carried out at the discharged state, and the corresponding Nyquist plots are shown in **Figure 5**a. The semi-circle indicates the combined interfacial resistance and charge transfer resistance at both cathode and anode.[33] The advantage of MC48-CNT as a cathode can be seen by comparing the spectra from S@P-CNT//Li and S@MC48-CNT//Li since both have the same lithium metal anode. At the tenth cycle, S@MC48-CNT//Li showed a smaller combined resistance of ≈70 Ω compared to ≈300 Ω of S@P-CNT//Li, suggesting MC48-CNT provides more favorable charge transfer and less interfacial resistance. The difference in the high-frequency intercepts on the real axis at 10th and 50th cycles, which could indicate the change in the electrolyte resistance, was found to be ≈20 Ω for S@MC48-CNT//Li and ≈50 Ω for S@P-CNT//Li. The smaller change in the electrolyte resistance with MC48-CNT could be attributed to less polysulfides in the electrolyte,[9b] as confirmed by the color change of the polysulfide solution and the smaller UV–vis intensity corresponding to the polysulfide with MC48-CNT compared to P-CNT (Figure 2c).

On the other hand, the favorable influence of MC48-CNT on the anode performance can be found by comparing the impedance spectra of S@MC48-CNT//Li and S@MC48-CNT//Li@MC48-CNT. Since the cathodes are same, the difference is supposed to originate from the anode side (i.e., pure lithium metal vs. lithium-infused MC48-CNT). A remarkable reduction of the combined interfacial and charge transfer resistance was observed from Li@MC48-CNT, which could be ascribed to improved lithium depositing and stripping kinetics due to the larger surface area for charge transfer

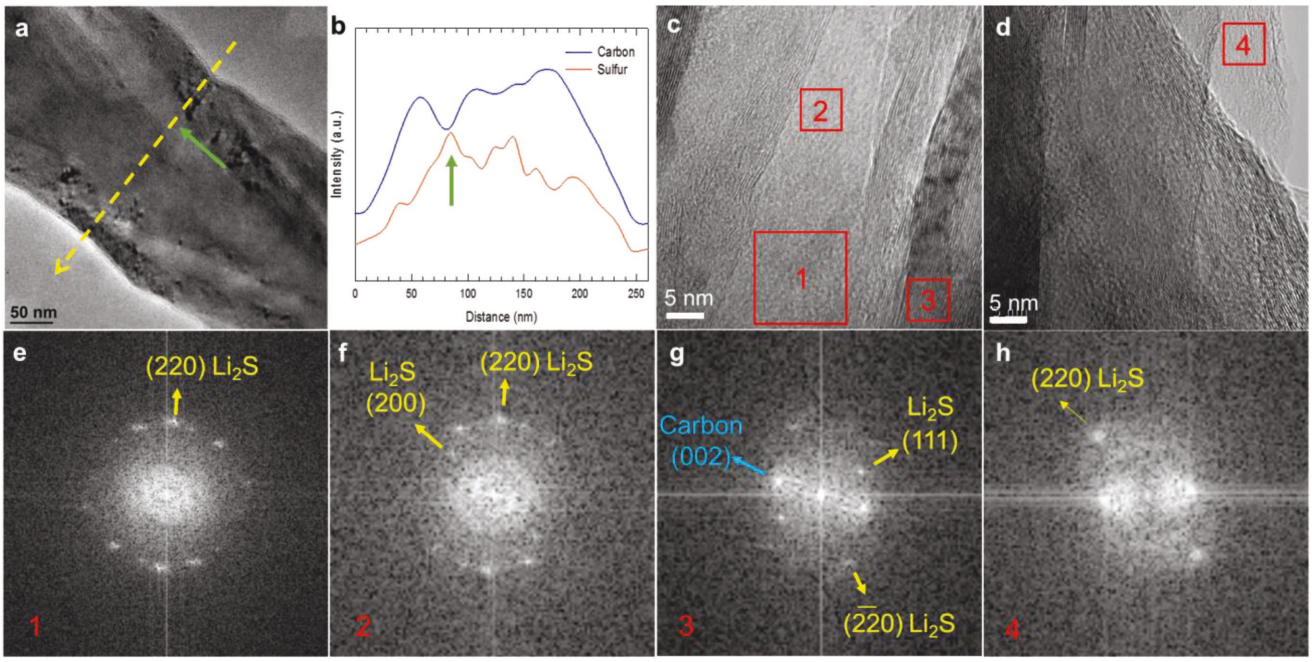

Figure 4. The mechanochemically treated MC48-CNT cathode after cycling. TEM images of S@MC48-CNT (cathode) a) after cycling and b) corresponding EDS line scan results. The green arrows in (a) and (b) indicate a trench where the intensity of carbon was lowered and that of sulfur was increased. High-resolution TEM images near c) a trench and d) an outer surface of S@MC48-CNT (cathode) after cycling. e–h) Fourier transformation of spots 1–4, showing the diffraction patterns of Li_2S and graphitic carbon.

and the lithiophilic surface of the functionalized CNT after the treatment.

The charge/discharge profiles at a high current density of 16 mA cm^{-2} were compared to clearly identify the effectiveness of the mechanochemically treated CNT electrode (Figure 5b). The smaller overpotential from S@MC48-CNT//Li compared with that of the pristine CNT (S@P-CNT//Li) indicates improved kinetics in cathode, and, for anode, S@MC48-CNT//Li@MC48-CNT suppressed the overpotential of Li metal (S@MC48-CNT//Li). The outstanding performance with the mechanochemical treatment (MC48-CNT) was manifested by the reduced overpotentials due to the synergistic improvement in the reaction kinetics at both cathode and anode. It should be noted that such a high current charge/discharge density significantly raises the overpotential, and it becomes even larger when the areal loading of active materials (sulfur) is high because of suppressed charge transfer on the electrode surface.

The relatively large overpotential from S@P-CNT//Li would have resulted in the large reduction in the capacity when the current density was increased from 1.6 to 16 mA cm^{-2} (Figure 5c). The largely reduced capacity from S@P-CNT//Li at 16 mA cm^{-2} was recovered when the mechanochemical CNT cathodes (S@MC11-CNT//Li and S@MC48-CNT//Li) were used. When MC48-CNT was used for both cathode and anode (S@MC48-CNT//Li@MC48-CNT), even after the current density was raised ten times, the areal capacity was slightly decreased from 13.3 to 11.0 mAh cm^{-2} (only ≈17% reduction), which is the highest areal capacity ever reported at this high charge/discharge current density, to the best of our knowledge.

As the large capacity improvement by MC48-CNT anode indicates the lithiophilic and porous host is essential to achieving high "power" performance (i.e., high power = voltage × high current), its performance as a lithium host was further tested with an asymmetric cell configuration (Li//MC48-CNT) used for typical anode performance testing. This cell showed a very stable cycling performance with a high areal capacity of 10–12 mAh cm^{-2} for more than 900 cycles at an extremely high areal current density of 31.3 mA cm^{-2} (Figure 5d). The outstanding performance could be attributed to more uniform deposition of lithium on the lithiophilic surface and the porous sponge structure accommodating the volume change associated with lithium deposition and stripping. The initial capacity increase is likely to be an activation process when lithium was incorporated into the bare trench–wall CNT host (i.e., no lithium at the beginning) in an electrochemical way (during charging), which is absent in the full cell testing with the anode whose lithium was thermally infused before testing.

The electrochemical performance of Li@MC48-CNT anode was further analyzed using a cell made of two symmetric Li@MC48-CNT electrodes in comparison to that of a symmetric lithium metal cell. Figure 5e depicts the voltage profiles at 8.3 mA cm^{-2} when cycled by limiting the capacity to 41.5 mAh cm^{-2}. The voltage plateau of Li@MC48-CNT was maintained to be less than ≈50% of that from the lithium metal cell for over 1700 h, indicating high stability and lower overpotentials.

3. Conclusions

A unique 3D trench–wall CNT framework was developed as effective free-standing sulfur/lithium dual hosts. This work simultaneously tackles the most crucial challenges in both

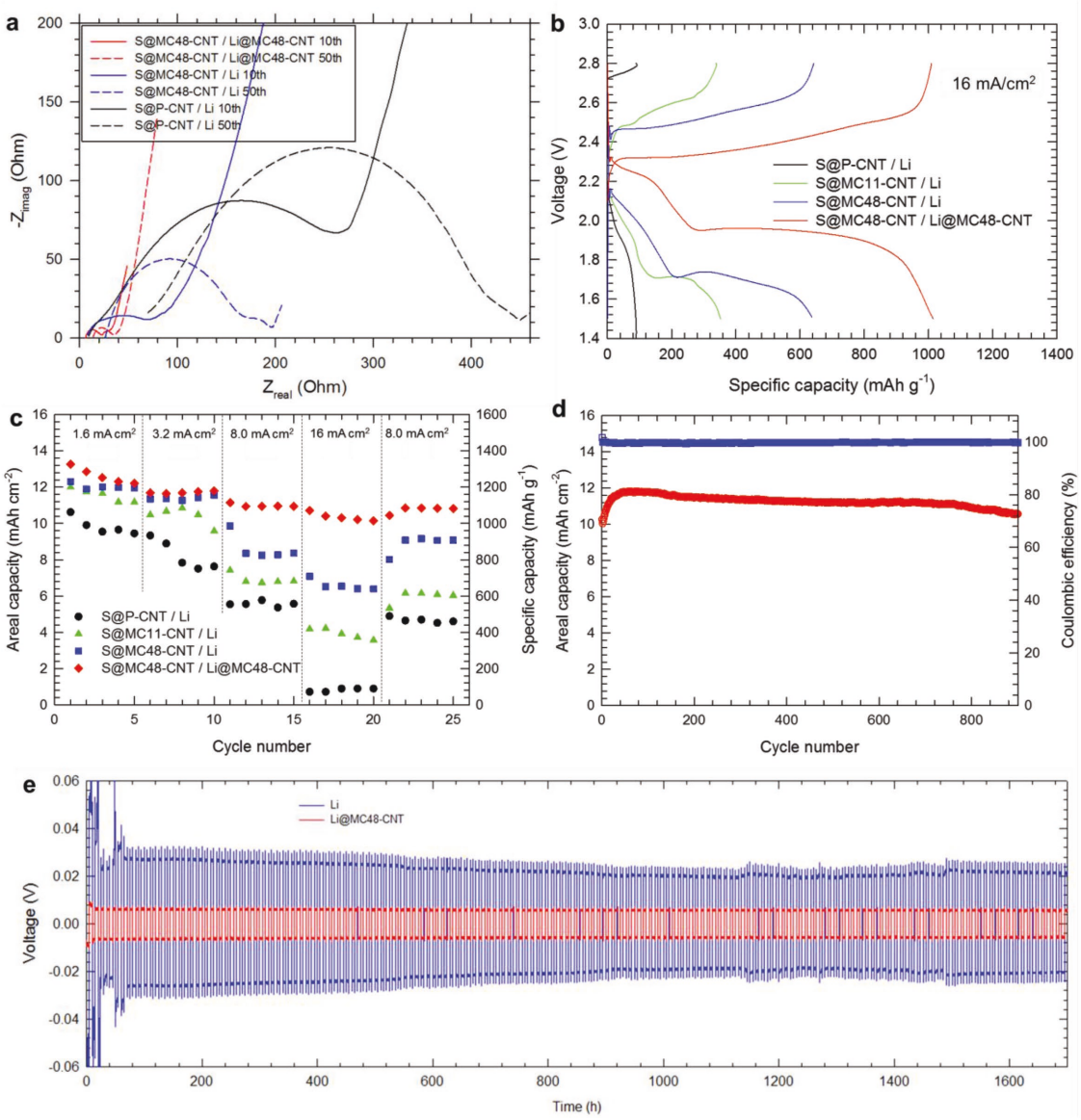

Figure 5. a) Nyquist plots of S@P-CNT//Li, S@MC48-CNT//Li, and S@MC48-CNT//Li@MC48-CNT at the 10th and 50th cycles. b) Voltage profiles of S@P-CNT//Li, S@MC11-CNT//Li, S@MC48-CNT//Li, and S@MC48-CNT//Li@MC48-CNT at a current density of 16 mA cm^{-2}. c) Rate capabilities of the Li-S cells at different cycling rates from 1.6 to 16 mA cm^{-2}. d) Cycling performance of the asymmetric cell, Li//MC48-CNT at a current density of 31.3 mA cm^{-2}. e) Voltage profiles of the two symmetric cells, Li//Li and Li@MC48-CNT//Li@MC48-CNT at a current density of 8.3 mA cm^{-2}.

cathode and anode in order to achieve a high "cell"-level energy density and power for practical Li-S batteries by increasing the areal loading of sulfur rather than only the specific capacity based on the sulfur mass. The key to achieving the striking improvement is the unique nanotrenches on the wall of CNTs, which were created without collapsing the free-standing CNT sponge structure using facile and controllable mechanochemical method. The nanotrenches became highly polysulfide-philic and lithiophilic, impeding the polysulfide shuttle especially for a high areal loading of sulfur as well as improving lithium deposition/stripping. A large reduction in the overpotentials during charge/discharge and improved kinetics would have resulted in the strikingly high areal capacity as high as 13.3 mAh cm^{-2} at an areal current density of 1.6 mA cm^{-2}, and maintained at 11.0 mAh cm^{-2} even with tenfold increase in the current density (16 mA cm^{-2}), suggesting both high "cell-level" energy density and power. This result shows that the trench–wall CNT can be an excellent host material for both cathode and anode, bringing Li-S batteries one step further toward practical applications along with the manufacturing-friendly sulfur-sandwiched cathode, and the dual-host design could be utilized in other rechargeable batteries with similar charge/discharge mechanisms.

4. Experimental Section

Preparation of the CNT Sponge: A cylindrical P-CNT sponge was grown by a chemical vapor deposition process[8] and then it was cut into coin-shape pieces with a thickness of ≈1 mm. For the chemical treatment,

a solution was prepared by dissolving $KMnO_4$ (AMRESCO, >99%) in sulfuric acid (BDH Chemicals, 95–98%) (0.5 g of $KMnO_4$ per liter of sulfuric acid). The mechanochemical process was performed with a typical vacuum filtration setup by adding the exfoliating agent drop wise on top of the CNT sponge placed on a glass filter, while controlling the vacuum pressure to obtain different trench features. The weight ratio of $KMnO_4$ to the CNT sponge was 1:2. To get rid of residual $KMnO_4$ and H_2SO_4, the CNT sponge was rinsed with deionized water and then ethanol (EMD Millipore, 95%). Finally, the CNT sponge was dried at 80 °C overnight.

Preparation of the Sandwich-Type Cathode: Solid sulfur powders (Alfa Aesar, 99.5%) were sprinkled on top of one piece of the CNT sponge with an areal sulfur loading of 10 mg cm^{-2}, and then another piece of the sponge was placed on the sulfur. The sulfur-sandwiched sponges were pressed under ≈50 MPa to make a free-standing cathode.

Preparation of the Li-Infused CNT Anode: A piece of lithium metal (Alfa Aesar, 99.9%) was cut and placed on top of a stainless steel sheet whose temperature was raised to 210 °C on a hot plate in an Ar-filled glove box (oxygen and moisture <0.1 ppm). The molten lithium was spontaneously infused into the CNT sponge when they were in contact. The infusion process was stopped by separating them when lithium fully covered the sponge.

Coin Cell Assembly and Test: 2032 coin-type cells were used for all tests. The full cells were assembled with the sulfur-sandwiched cathode and the Li-infused CNT sponge anode or the pure lithium metal (Alfa Aesar, 99.9%) anode along with a Celgard 2400 separator (5/8 in. in diameter). The diameter of cathode was 3/8 in. and that of anode was 1/2 in. The sulfur loading is based on the area of the cathode. The symmetric cells were assembled with the Li-infused CNT sponge or pure lithium metal. The asymmetric cells were assembled with the mechanochemically treated CNT cathode and lithium metal anode. The electrolyte (1 M LiTFSI (Sigma-Aldrich, 99%) and 0.5 M $LiNO_3$ (Alfa Aesar, 99%) in a mixture of 1,3-dioxolane (Alfa Aesar, 99.5%) and 1,2-dimethoxyethane (Alfa Aesar, 99+%) (1:1 by vol.)) amount was 5 µL per milligram of sulfur. The battery tests were carried out with the Arbin BT2000 or Landt CT2001 galvanostat. The cycling tests of the full cells were started with 0.32 mA cm^{-2} for activation and then cycled at 4.8 mA cm^{-2} between 1.7 and 2.8 V. The symmetric cells were cycled by limiting the charge and discharge capacity to 41.5 mAh cm^{-2} at a current density of 8.3 mA cm^{-2}. The asymmetric cells were cycled between 0 and 2 V at a current density of 31.3 mA cm^{-2}.

Supporting Information

Supporting Information is available from the Wiley Online Library or from the author.

Acknowledgements

The authors gratefully ackonlwedge financial support from the U.S. National Science Foundation (IIP 1701200 and 1655429).

Conflict of Interest

The authors declare no conflict of interest.

Keywords

carbon nanotubes, Li-S batteries, mechanochemical treatments, sponges, surface modification

Received: January 23, 2018
Revised: March 28, 2018
Published online: June 14, 2018

[1] J. Lu, Z. H. Chen, Z. F. Ma, F. Pan, L. A. Curtiss, K. Amine, *Nat. Nanotechnol.* **2016**, *11*, 1031.
[2] a) P. G. Bruce, S. A. Freunberger, L. J. Hardwick, J. M. Tarascon, *Nat. Mater.* **2012**, *11*, 19; b) H. J. Peng, J. Q. Huang, X. B. Cheng, Q. Zhang, *Adv. Energy Mater.* **2017**, *7*, 1700260.
[3] a) X. L. Ji, K. T. Lee, L. F. Nazar, *Nat. Mater.* **2009**, *8*, 500; b) Q. Pang, X. Liang, C. Y. Kwok, L. F. Nazar, *Nat. Energy* **2016**, *1*, 16132; c) A. Manthiram, Y. Z. Fu, S. H. Chung, C. X. Zu, Y. S. Su, *Chem. Rev.* **2014**, *114*, 11751; d) Y. X. Yin, S. Xin, Y. G. Guo, L. J. Wan, *Angew. Chem., Int. Ed.* **2013**, *52*, 13186; e) S. H. Chung, P. Han, C. H. Chang, A. Manthiram, *Adv. Energy Mater.* **2017**, *7*, 1700537; f) G. Hu, Z. Sun, C. Shi, R. Fang, J. Chen, P. Hou, C. Liu, H. M. Cheng, F. Li, *Adv. Mater.* **2017**, *29*, 1603835.
[4] a) D. Lv, J. Zheng, Q. Li, X. Xie, S. Ferrara, Z. Nie, L. B. Mehdi, N. D. Browning, J.-G. Zhang, G. L. Graff, J. Liu, J. Xiao, *Adv. Energy Mater.* **2015**, *5*, 1402290; b) M. A. Pope, I. A. Aksay, *Adv. Energy Mater.* **2015**, *5*, 1500124; c) J. Song, Z. Yu, M. L. Gordin, D. Wang, *Nano Lett.* **2016**, *16*, 864; d) W. Zhou, B. Guo, H. Gao, J. B. Goodenough, *Adv. Energy Mater.* **2016**, *6*, 1502059.
[5] J. B. Goodenough, Y. Kim, *Chem. Mater.* **2010**, *22*, 587.
[6] a) W. Xu, J. L. Wang, F. Ding, X. L. Chen, E. Nasybutin, Y. H. Zhang, J. G. Zhang, *Energy Environ. Sci.* **2014**, *7*, 513; b) K. Zhang, G. H. Lee, M. Park, W. J. Li, Y. M. Kang, *Adv. Energy Mater.* **2016**, *6*, 1600811; c) D. C. Lin, Y. Y. Liu, Y. Cui, *Nat. Nanotechnol.* **2017**, *12*, 194.
[7] a) H. Ota, K. Shima, M. Ue, J. Yamaki, *Electrochim. Acta* **2004**, *49*, 565; b) Y. Matsuda, T. Takemitsu, T. Tanigawa, T. Fukushima, *J Power Sources* **2001**, *97–98*, 589; c) J. F. Qian, W. A. Henderson, W. Xu, P. Bhattacharya, M. Engelhard, O. Borodin, J. G. Zhang, *Nat. Commun.* **2015**, *6*, 6362; d) Q. C. Liu, J. J. Xu, S. Yuan, Z. W. Chang, D. Xu, Y. B. Yin, L. Li, H. X. Zhong, Y. S. Jiang, J. M. Yan, X. B. Zhang, *Adv. Mater.* **2015**, *27*, 5241; e) G. Y. Zheng, S. W. Lee, Z. Liang, H. W. Lee, K. Yan, H. B. Yao, H. T. Wang, W. Y. Li, S. Chu, Y. Cui, *Nat. Nanotechnol.* **2014**, *9*, 618; f) K. Yan, H. W. Lee, T. Gao, G. Y. Zheng, H. B. Yao, H. T. Wang, Z. D. Lu, Y. Zhou, Z. Liang, Z. F. Liu, S. Chu, Y. Cui, *Nano Lett.* **2014**, *14*, 6016; g) P. Liu, Q. Ma, Z. Fang, J. Ma, Y. S. Hu, Z. B. Zhou, H. Li, X. J. Huang, L. Q. Chen, *Chin. Phys. B* **2016**, *25*, 078203; h) X. B. Cheng, R. Zhang, C. Z. Zhao, F. Wei, J. G. Zhang, Q. Zhang, *Adv. Sci.* **2016**, *3*, 1500213; i) Y. Y. Liu, D. C. Lin, P. Y. Yuen, K. Liu, J. Xie, R. H. Dauskardt, Y. Cui, *Adv. Mater.* **2017**, *29*, 1605531.
[8] G. Yang, W. Choi, X. Pu, C. Yu, *Energy Environ. Sci.* **2015**, *8*, 1799.
[9] a) X. Pu, G. Yang, C. Yu, *Adv. Mater.* **2014**, *26*, 7456; b) X. Pu, G. Yang, C. Yu, *J. Electrochem. Soc.* **2015**, *162*, A1396.
[10] Z. W. Seh, Q. F. Zhang, W. Y. Li, G. Y. Zheng, H. B. Yao, Y. Cui, *Chem. Sci.* **2013**, *4*, 3673.
[11] D. V. Kosynkin, A. L. Higginbotham, A. Sinitskii, J. R. Lomeda, A. Dimiev, B. K. Price, J. M. Tour, *Nature* **2009**, *458*, 872.
[12] D. Lin, Y. Liu, Z. Liang, H.-W. Lee, J. Sun, H. Wang, K. Yan, J. Xie, Y. Cui, *Nat. Nano* **2016**, *11*, 626.
[13] X. Pu, G. Yang, C. Yu, *Nano Energy* **2014**, *9*, 318.
[14] T. Chen, B. R. Cheng, G. Y. Zhu, R. P. Chen, Y. Hu, L. B. Ma, H. L. Lv, Y. R. Wang, J. Liang, Z. X. Tie, Z. Jin, J. Liu, *Nano Lett.* **2017**, *17*, 437.
[15] S. H. Chung, C. H. Chang, A. Manthiram, *Energy Environ. Sci.* **2016**, *9*, 3188.
[16] X. Liang, Y. Rangom, C. Y. Kwok, Q. Pang, L. F. Nazar, *Adv. Mater.* **2017**, *29*, 1603040.
[17] H. J. Peng, W. T. Xu, L. Zhu, D. W. Wang, J. Q. Huang, X. B. Cheng, Z. Yuan, F. Wei, Q. Zhang, *Adv. Funct. Mater.* **2016**, *26*, 6351.
[18] X. B. Cheng, H. J. Peng, J. Q. Huang, L. Zhu, S. H. Yang, Y. Liu, H. W. Zhang, W. C. Zhu, F. Wei, Q. Zhang, *J. Power Sources* **2014**, *261*, 264.
[19] Z. Yuan, H. J. Peng, J. Q. Huang, X. Y. Liu, D. W. Wang, X. B. Cheng, Q. Zhang, *Adv. Funct. Mater.* **2014**, *24*, 6105.
[20] G. M. Zhou, L. Li, C. Q. Ma, S. G. Wang, Y. Shi, N. Koratkar, W. C. Ren, F. Li, H. M. Cheng, *Nano Energy* **2015**, *11*, 356.

[21] H. J. Peng, Z. W. Zhang, J. Q. Huang, G. Zhang, J. Xie, W. T. Xu, J. L. Shi, X. Chen, X. B. Cheng, Q. Zhang, *Adv. Mater.* **2016**, *28*, 9551.
[22] G. J. Hu, C. Xu, Z. H. Sun, S. G. Wang, H. M. Cheng, F. Li, W. C. Ren, *Adv. Mater.* **2016**, *28*, 1603.
[23] R. P. Fang, S. Y. Zhao, S. F. Pei, X. T. Qian, P. X. Hou, H. M. Cheng, C. Liu, F. Li, *ACS Nano* **2016**, *10*, 8676.
[24] W. G. Chong, J. Q. Huang, Z. L. Xu, X. Y. Qin, X. Y. Wang, J. K. Kim, *Adv. Funct. Mater.* **2017**, *27*, 1604815.
[25] Q. Pang, X. Liang, C. Y. Kwok, J. Kulisch, L. F. Nazar, *Adv. Energy Mater.* **2017**, *7*, 1601630.
[26] Z. Li, J. T. Zhang, Y. M. Chen, J. Li, X. W. Lou, *Nat. Commun.* **2015**, *6*, 8850.
[27] M. Li, Y. N. Zhang, X. L. Wang, W. Ahn, G. P. Jiang, K. Feng, G. Lui, Z. W. Chen, *Adv. Funct. Mater.* **2016**, *26*, 8408.
[28] H. Q. Wang, W. C. Zhang, H. K. Liu, Z. P. Guo, *Angew. Chem., Int. Ed.* **2016**, *55*, 3992.
[29] S. H. Chung, C. H. Chang, A. Manthiram, *Small* **2016**, *12*, 939.
[30] J. Liu, D. G. D. Galpaya, L. J. Yan, M. H. Sun, Z. Lin, C. Yan, C. D. Liang, S. Q. Zhang, *Energy Environ. Sci.* **2017**, *10*, 750.
[31] L. Qie, A. Manthiram, *Adv. Mater.* **2015**, *27*, 1694.
[32] L. X. Miao, W. K. Wang, K. G. Yuan, Y. S. Yang, A. B. Wang, *Chem. Commun.* **2014**, *50*, 13231.
[33] a) G. Bieker, M. Winter, P. Bieker, *Phys. Chem. Chem. Phys.* **2015**, *17*, 8670; b) Z. F. Deng, Z. A. Zhang, Y. Q. Lai, J. Liu, J. Li, Y. X. Liu, *J. Electrochem. Soc.* **2013**, *160*, A553; c) N. A. Canas, K. Hirose, B. Pascucci, N. Wagner, K. A. Friedrich, R. Hiesgen, *Electrochim. Acta* **2013**, *97*, 42; d) S. Risse, N. A. Canas, N. Wagner, E. Hark, M. Ballauff, K. A. Friedrich, *J. Power Sources* **2016**, *323*, 107.